N89-13317

Application of PN and Avalanche Silicon Photodiodes to Low-Level Optical Radiation Measurements.

G. Eppeldauer* and A.R. Schaefer

National Bureau of Standards

Gaithersburg, Maryland 20899 USA

ABSTRACT

New approaches to the discovery of other planetary systems require very sensitive and stable detection techniques in order to succeed. Two methods in particular, the astrometric and the photometric methods, require this. To begin understanding the problems and limitations of solid state detectors, particularly silicon photodiodes, regarding this application; preliminary experiments have been performed at NBS and a low light level detector characterization facility was constructed. We will briefly describe this facility, and outline the results of tests conducted with it. We will then describe a breadboard photometer which was built at NBS and used at Lick Observatory to obtain stellar brightness ratio precision data. The remainder of the paper will be devoted to a discussion of design principles of PN and avalanche silicon photodiode based low light level measuring circuits. An emphasis is placed on obtaining maximum sensitivity using optimum detectors and transimpedance amplifiers. We discuss the effects of shunt impedance, noise sources, and thermal effects. A comparison is made between ordinary and avalanche devices for this particular type of measurement.

*Guest worker from the Research Institute for Technical Physics of the Hungarian Academy of Sciences, Budapest, Hungary.

PRECEDING PAGE BLANK NOT FILMED

1. Introduction

Detection of extrasolar planetary systems is important to the understanding of star formation, the formation of planetary systems, and to the estimation of how common life is throughout the universe. Several techniques are being pursued currently in the endeavor to find new planetary systems. Two of the more promising approaches to searching for other planetary systems which are currently being investigated, the astrometric method and the photometric method, require very sensitive and stable detectors in order to succeed.

The simplest photometric method of searching for planets around stars depends on observing the decrease in starlight produced by the transit of a planet across the stellar disk. The magnitude of this reduction is proportional to the ratio of the planet's area to that of the star. For the solar system, the decrease in light amounts to one percent for a giant planet such as Jupiter and Saturn, 0.1 percent for planets the proportions of Uranus and Neptune, and 0.01 percent for terrestrial-sized planets (Borucki and Summers, 1984; Borucki, 1984). Figure 1, for example, shows a calculation of the flux variation as a function of time as a Jupiter sized planet crosses the Sun. To make certain that a transit would be clearly distinguished from noise fluctuations, it is necessary to operate with a high signal to noise ratio (SNR). Consequently, the photometer should produce a SNR of approximately 10 for the dimmest stars that will be monitored.

In order to detect 1 part in 10^4 variation of a star's brightness due to a transit by an Earth-sized planet, it is necessary to insure that signal variations due to other sources do not overwhelm the transit signal. Three sources of error can be identified; variability of the star itself, instrument problems such as detector/amplifier instabilities, and variations of the stellar light flux due to atmospheric variability. The purpose of the work described in this paper is to begin to understand the limitations due to detector/amplifier capabilities.

Research has demonstrated that high quantum efficiency photodiodes can be applied quite effectively to the planetary search problem. Schaefer (1984) presented a review of the applicability of solid state photodiodes to stellar radiometric measurements. This review pointed out the work at NBS (Zalewski and Geist, 1980, Geist, Zalewski, and Schaefer, 1980, and Geist, Liang, and Schaefer, 1981) which displayed the techniques and applications of silicon photodiodes having one hundred percent internal quantum efficiency. It was also mentioned that Fisher (1968) has discussed the possible advantages of using solid state detectors in astronomical radiometric measurements. He noted the advantages of the much higher quantum efficiency of silicon diodes and their larger range of linearity compared to photomultipliers.

In the review (Schaefer, 1984) it was noted that gallium arsenide phosphide (GaAsP) detectors may offer even more promise for such applications. Wilson and Lyall (1986) have noted the advantages of GaAsP

devices over silicon photodiodes: specifically, they have higher shunt impedance, which makes possible their use with higher feedback resistances in their transimpedance amplifiers without sacrificing performance in noise or linearity. These devices typically have a large junction capacitance. Noise performance in a photodiode is dominated by the Johnson noise for the shunt impedance of the photodiode and the interaction of the amplifier voltage noise with the input capacitance and resistance. The larger capacitance of GaAsP results in increased noise due to the interaction with amplifier voltage noise; however, since the shunt impedance for GaAsP devices is several orders of magnitude larger than silicon, noise performance should still be superior to that of silicon if a low measurement bandwidth (less than 1 Hz) can be tolerated. This is the case for the planetary measurements being discussed.

2. Low Light Level Detector Characterization Facility

In Figure 2 we show a block diagram of the low light level detector characterization facility which was constructed at NBS. This optical table was constructed in such a manner as to provide thermal, vibrational, and optical isolation for testing of high sensitivity detectors and amplifiers. The facility consists of a four by six foot vibrationally damped optical table on vibration isolating pneumatic legs. On this base table is an unrestrained two by four foot invar table top which provides dimensional stability even if the ambient temperature undergoes a considerable change. The table is enclosed in a light proof

box, which actually consists of two parts: a sliding panel cover over the entire table, and a completely light-tight PVC box that covers the invar table top.

A variety of optical arrangements can be fashioned on the invar table. For the work described, a low light level tritium phosphorescent source was mounted as shown behind an electrically controlled shutter and an adjustable aperture. A multiple detector holding post was positioned at the opposite end of the table. The detector photocurrents passed through transimpedance amplifiers, and then to digital multimeters for measuring and recording. The experiments were controlled by a microcomputer that could command the data acquisition from up to four simultaneously triggered multimeters (three for detector outputs, and one for temperature.) The temperature was monitored via a thermistor mounted on the detector or amplifier housing, depending on the test being done.

In addition, a very high gain, stable two stage transimpedance amplifier with three channels was constructed and tested. This device consisted of a FET current to voltage converter with a second stage resistor attenuator and buffer. The total gain of these amplifiers was 10^{11} V/A.

A number of preliminary screening tests were run on various silicon and gallium arsenide phosphide diodes. Several devices were selected based on their noise performance and stability for use in further studies.

Figure 3, 4, and 5 display some typical results using a high quality pair of silicon photodiodes whose photocurrents are amplified by the amplifier just described. During the first 300 minutes, the temperature of the transimpedance amplifier was dropped from 0 to -20 °C and back again, which is responsible for the small drift at the beginning of the individual channel curves. One can note; however, that the ratio of the two signals does not drift, and the standard deviation of a reading (each of which represents four minutes of integration) is only 0.13%

3. Breadboard Photometer

In order to further establish the potential of silicon photodiodes in such applications, and to provide ground based tests for different types of detectors, preamps, and optical components, a breadboard photometer was designed by Schaefer and Borucki, fabricated at NBS, and tested at NBS and Lick Observatory on the 19 inch Twin Astrograph telescope. Figure 6 shows a diagram of the system. The telescope tests are described by Borucki et al (1987). The photometer consisted of a plate which could be inserted into the telescope. This plate contained a rotatable wheel with slots, such that three detectors could be positioned anywhere within the focal plane of the telescope. Each of the three detectors had its own high gain (10^{11}) transimpedance amplifier. These three channels were used to simultaneously monitor two stars and the sky. Analog to digital conversion and signal averaging were again done with digital multimeters controlled by a microcomputer.

The system was tested at NBS using Hamamatsu silicon photodiodes of $1mm^2$ light sensitive area and 5 mm external diameter. Each of the three channels measured the light output from the highly stable, tritium activated phosphorescent source. By correlating relative drift among the three channels, it was established that relative flux ratios could be determined with a precision of better than 0.1 % using four minute integration times.

Next, the system was installed on the Lick Observatory twin astrograph. Figure 7 shows some data obtained on α and β Aries with the breadboard photometer. The top two strips show the output from each of the two channels monitoring the stars after corrections for the sky background, the detector dark currents, and for the extinction due to the changes in the air mass with time. It is clear that during the approximately 3 hour observational period, the extinction per air mass has changed by about 1 %. The ratio of the fluxes from the two stars is shown in the bottom strip. The significant improvement in the measurement precision is clear. The top two records have a standard deviation of 4.5×10^{-3} whereas the ratio has a standard deviation of 5×10^{-4}. For solar-type stars, the precision obtained during this test is sufficient to detect Jupiter-sized or Uranus-sized planets with SNR's of 20 and 2, respectively. Although the precision demonstrated by the breadboard photometer is too low to search for Earth-sized planets, the significant increase in precision over conventional photometers is encouraging.

The results obtained up to this point are very encouraging. Ground-based searches for Jupiter or Neptune sized planets will actually become feasible once instrumentation is developed to monitor a sufficient number of stars simultaneously at a precision of one part in 10,000. Furthermore, these improvements in photometric instrumentation should also significantly impact other areas of astronomical research; for example: measurements of low-level stellar variability, determination of asteroid properties, and the recognition of low contrast features in planetary atmospheres and on planetary surfaces.

4. PN Silicon Photodiodes

For high sensitivity non-imaging light measurements, large area photovoltaic detectors should be used. High quality photovoltaic detectors have quantum efficiencies near to unity. Bhardwaj (1982) reported that their dominant noise is thermal noise as they do not need biasing voltages. The most critical electrical parameter of large area photovoltaic detectors is their shunt resistance.

Table 1 shows several dark shunt resistance measurement results as a function of temperature determined on several high quality photovoltaic detectors.

It can be seen, that the shunt resistance can vary several orders of magnitude depending on detector type and individual properties. The Table also shows that the shunt resistance is strongly temperature

dependent and that the temperature coefficient of shunt resistance varies from detector to detector. As the zero error of the light measuring circuit will depend on the shunt resistance of the photovoltaic detector, it follows that for accurate measurements, the photovoltaic detectors have to be kept at a constant temperature. As will be shown later, to achieve high sensitivity the shunt resistance of the detector should be high. The minimum shunt resistance that can be used, depends on the design of the light measuring circuit as well.

For non-imaging radiation (illumination) measurements the short circuit current also depends on the cell area. Therefore, for very high sensitivity applications the light sensitive area should be large. However, the larger the surface the lower the shunt resistance. With present day technology a 1 cm^2 area seems to be a good compromise. The current-voltage characteristic of a 1 cm^2 surface Hamamatsu photovoltaic detector Model 1227-1010BQ is shown in Fig. 8. It has a shunt resistance at least as large as 1.95×10^9 ohm.

5. Amplifiers

The electrical output signal of high quality photovoltaic detectors changes linearly with input light flux over a very wide range provided that their short circuit current is correctly measured. Eppeldauer and Lanc (1980) showed that electronic circuits with high quality operational amplifiers have to be used to achieve this. Table 2 shows several operational amplifiers that are suitable for measuring the short circuit

photodetector current even if it is less than 10^{-13} A. All the amplifiers in the first five groups are ultra low bias current FET input electrometer operational amplifiers. The amplifiers in the last two groups are dielectrically isolated FET operational amplifiers. Columns 2 through 5 show the manufacturer's specifications for those parameters that are most important for low current measurement. As Eppeldauer (1982) discussed earlier the low frequency 1/f noise in the low electrical frequency range is the dominant error component for such a short circuit current to voltage converter. Unfortunately, the low frequency input noise voltage differs even for similar operational amplifiers. This is illustrated in Fig. 9 where the low frequency voltage noise of 27 AD 515 and BB 3523 operational amplifiers is compared in the frequency band from 0 to 0.1 Hz. The measured noise can change more than 1 order of magnitude even if operational amplifiers of equivalent types are used. Note that the amplifier temperature was held at 35°C during the noise measurements reported in Fig. 9.

Similar differences were obtained when the low frequency voltage noise of four OPA 111 AM operational amplifiers were measured at the same temperature. The results are shown in Table 3.

It can be seen by comparison of Fig. 2 and Table 3 that the newly developed OPA 111 dielectrically-isolated FET operational amplifier has a significantly lower low frequency 1/f noise than the ultra low bias current FET input electrometer operational amplifiers.

6. Light measuring circuits

In order to determine the most important output error components of the light measuring circuit, first the simplified equivalent circuit has to be examined. This circuit is shown in Fig. 10.

The real operational amplifier can be replaced by an ideal one, where voltage and current generators are coupled to the input of the ideal amplifier, representing both DC voltage and current drifts. Also, voltage and current noises are represented if the voltages and currents are thought of as general instantaneous error sources. The difference between the DC and noise errors is that the latter cannot be predicted as a function of time. It is a random variable and must be described in probabilistic terms. The internal noise sources of operational amplifiers are normally uncorrelated. This means that they are randomly related to each other in time and there is no systematic phase relationship. These uncorrelated noise quantities are combined in quadrature. The resultant input voltage noise of the operational amplifier can thus be written in the following form:

$$V_{rn} = \left[V_n^2 + (I_n \cdot R_r)^2 + 4 \cdot k \cdot T \cdot R_r \cdot \Delta f \right]^{1/2} \qquad (1)$$

where the source resistance is:

$$R_r = \frac{R_f \cdot R_s}{R_f + R_s} \qquad (2)$$

V_n and I_n are the voltage and current noises of the operational amplifier, k = 1.38 . 10^{-23} J/K and T = 298 K. The frequency dependence of V_n and I_n will be discussed in detail later in this paper. Because manufacturers' data usually deal only with V_n and I_n above 0.1 Hz, the discussion of Eq. 1 will be carried out for two frequency ranges: Δf1 and Δf2 respectively, where Δf2 = 0 to 0.1 Hz and Δf1, = 0.1 Hz to 10 Hz.

In the Δf1=0.1 to 10 Hz frequency range the voltage and current noises can be found in the manufactures data sheets. First the voltage and current noises were calculated only for operational amplifiers of 3523 type (shown in Table 2).

In the Δf2=0 to 0.1Hz range the values of the voltage and current noise are not contained in the manufacturers' data sheets. Therefore, we measured the total nosise in this frequency range. Recorded output voltages of the operational amplifier 3523 type are shown in Fig. 11 with source resistance as a parameter (see Eqn. 2 & 3). During all measurements the amplification was 50 and the value of the shunt resistance was changed by factors of ten from 100kΩ to 1 GΩ. The amplifier sensitivity setting of the plotter was constant for the lower values of resistance, while it was reduced by a factor of 2.5 for the highest resistance. The duration of the recording was 8.5 minutes in each case.

Similar measurements and calculations were performed for another type of operational amplifier (111 type in Table 2) as well. As shown in Fig. 12, the output voltages were measured at source resistance values from 1Mohm to 1GΩ for 7 minutes. The output sensitivity is 40μV/div and the amplification is 50 for each curve.

Fig. 13 and Fig. 14 show the input noise voltage characteristics of the two types of operational amplifiers as functions of the source resistance. As can be seen from Fig. 13 and 14, the very low frequency total noise can change in a wide range because of the differences among the individual operational amplifiers. When the electrical bandwidth is extended to 10 Hz the Johnson noise of the source resistance will dominate the noise characteristic if the value of the source resistance is higher than about 10 MΩ in the case of type 3523 operational amplifier and about 1 MΩ in the case of type 111 operational amplifier. In many practical applications high speed is not a requirement, therefore, at the output of the operational amplifier a low-pass filter with a 1.6 s time constant could be used, in which case only the 0 to 0.1 Hz electrical bandwidth contributes to the total noise. In this case the 1/f total noise would dominate the input characteristics. In the case of the 111 type operational amplifiers, as shown in Fig. 14, the voltage noise of the operational amplifier in both frequency ranges is lower than in case of operational amplifier 3523 type. The value of the source resistance is essentially the same as the value of the shunt resistance of the detector if the feedback resistor of the operational amplifier is

significantly higher than the shunt resistance of the detector. At about 1 GΩ source resistance the input noise voltages of the two different type of operational amplifiers are roughly equal.

The DC offset voltage and current also can cause error components in the output voltage of the operational amplifier. The amplification for both the DC and noise input errors depends on the value of the shunt resistance R_s of the photovoltaic detector and that of the feedback resistor R_f of the operational amplifier. The voltage amplification of the light measuring circuit shown as an inset in Fig. 15 and 16 is:

$$A = \frac{R_f + R_s}{R_s} \cdot \frac{9 + 1}{1} , \qquad (3)$$

and the two figures show the output zero voltages of type 3523 and 111 operational amplifiers as function of shunt resistance of photovoltaic detector, respectively.

The total noise output characteristic for both amplifier types was calculated in the frequency range between 0 and 0.1 Hz. They are derived from the input noise characteristics shown in Fig. 13 and 14. For the calculation of the DC output voltage errors we took into consideration that the temperature of the operational amplifiers were stabilized to within a range of 0.1°C.

These output characteristics can be used to choose the optimum combination of photovoltaic detector and operational amplifier to achieve a desired high sensitivity . For example, Figs. 15 and 16 show that similar output zero voltage error can be achieved with type 111 operational amplifier as with type 3523 operational amplifier provided that an order of magnitude lower detector shunt resistance is used with the type 111 operational amplifier. If the amplifiers are selected to achieve the lowest 1/f noise, the highest possible light sensitivity can be achieved with operational amplifier 3523 type provided that a photovoltaic detector of higher than 10^9 ohm shunt resistance is being used. If a photovoltaic detector of less than 10^9 ohm shunt resistance has to be used and the highest possible light sensitivity is to be obtained, then the type 111 operational amplifiers would be a better device.

Only the most sensitive range, which corresponds to a feedback resistor of 50 GΩ, was examined in the above analysis. This means that the transimpedance of the short circuit current to voltage converter was 50 mV/pA. If 10^{-14} A short circuit current is the minimum detectable current of interest, the resultant output zero errors have to be lower than 0.5 mV.

7. Temperature control

As can be seen in Table 1, the necessary shunt resistance can be obtained not only by selecting the proper type of detector, but also by

temperature control of the detector. The second task of the temperature control is to reduce the temperature drift of the photovoltaic cell and operational amplifier. The error of temperature stabilization is an important parameter which has to be known to calculate the DC errors at the output of the operational amplifier. Both heating and cooling type control loops can be used for temperature control. The former which generally utilizes a heating transistor is simpler and also is less expensive than the latter. Its disadvantage is that very high shunt resistance values cannot be obtained, because the controlled temperature must be higher than the temperature of the laboratory.

The advantage of the cooling type temperature control is that the temperature can be controlled in a wider range according to the required shunt resistance value of the photovoltaic detector. However, cooling the selected detector - operational amplifier pair below ambient temperature requires hermetical sealing for all the cooled components (including the input optics such as filters, etc.) to avoid water condensation on the surfaces. This requires more careful design, and more expensive mechanical and optical construction.

8. Measurement results

According to the above considerations we made combinations of several photovoltaic detectors and operational amplifiers and measured the output zero errors of the light measuring circuit (see Figs. 15 and 16) as a function of temperature. The duration of the measurements at each

temperature was 10 minutes. During this time one hundred measurements were made in the dark. Table 4 shows the measurement results when photovoltaic detector 1-A (see Table 1), which has a shunt resistance significantly lower than 1 GΩ, was matched to a type 111 operational ampilifier. The standard deviation from one hundred measurements was 0.25 mV at 25°C which means that the short circuit current error is a factor of two lower than the earlier mentioned 0.5 mV maximum allowed error for 10^{-14} A resolution.

As shown in Table 5, operational amplifier of type 111 was also used with another photovoltaic detector, 1-C, which has over 5 times the shunt resistance of the detector 1-A. It can be seen from Fig. 16 that at such high shunt resistances the output zero errors do not change significantly. Therefore, the standard deviation does not change with temperature. The measured highest sensitivity is shown in Table 6, where detector 1-C was matched with an operational amplifier of type 3523. Photovoltaic detector 1-C has sufficiently high shunt resistance to perform better with this type of operational amplifier, which is, in general, about 3 times more expensive than type 111 amplifiers. The output voltage standard deviation at 25°C was 0.07 mV which is 7 times smaller than the above mentioned 0.5 mV maximum allowed error for 10^{-14} A resolution. This means that the short circuit current sensitivity is 1.4 x 10^{-15}A. If we check the maximum to minimum error, it is 0.34 mV at 25°C, that is the peak to peak error is also less than the above mentioned 0.5 mV error.

9. Avalanche Silicon Photodiodes

The important characteristic of reverse biased avalanche photodiodes is that internal current gain is obtained from the multiplication of photogenerated carriers. Weak signals therefore, are raised to a detectable level above the amplifier noise.

We used the "reach-through" type devices where the reverse bias depletes the junction first, forming a high field multiplication region. Further bias causes the depletion to reach-through into the intrinsic region, and a little more voltage causes the device to be fully depleted up to the back contact. At voltages above this level an electric field in the intrinsic region is created which is sufficient to give high carrier velocities but not avalanche effects.

Unfortunately, the changes of ambient temperature result in changes of multiplication. Instead of ambient temperature dependent bias voltage adjustments, we used a temperature controlled housing for the diodes. The construction of the measuring head is shown in Fig. 17. This is a shielded multi-cavity arrangement which measures short circuit current according to Fig. 18. This circuit uses an electrometer operational amplifier. This is the same measuring head that was used for the previously discussed measurements of the PN silicon photodiodes.

RCA C30872 silicon avalanche photodiodes were measured in TO-8 packages. A modification according to Fig. 19 and 20 was constructed to

accommodate the avalanche diodes in the thermostated measuring head. Some additional electronic circuits were made and located within the design to perform the high voltage biasing according to Fig. 21. Avalanche photodiode D, was biased by the highly stable output voltage U_B of a regulatable high voltage power supply. The opposite polarity output voltage U_C of another power supply of the same type was used to produce a compensating current through resistor R at the inverting input of the operational amplifier, OA, to get zero output voltage U_O, when D is in the dark. The temperature of the Aluminum adapter and detector was controlled to 27.5°C ±0.1°C. In this way, the 2.2 V/°C temperature coefficient of the DC reverse operating voltage was eliminated.

First, electronic simulation measurements were made of the compensation of the high voltage bias and minimalization of the signal instabilities. For this purpose detector D and resistor R were substituted with high quality 1 GΩ metal oxide resistors. Both U_B and U_C were set to about 300 V. The standard deviation obtained of U_O was 0.3% during a 1 hour measurement. This result shows that in our case this minimum error is determined by the instabilities of the high voltage sources used. The specified instability of the high voltage sources was 0.01%. If lower standard deviation is necessary higher quality high voltage sources must be used.

We compared the measured sensitivity of the 3 mm diameter photosensitive area avalanche photodiode to the sensitivity obtained with 1 mm^2 photosensitive area PN silicon photodiodes. At 300V bias $R_F=10^8$ ohm gave almost as high U_O output as with the PN photodiode and a 10^{11} ohm feedback resistor. Similar output voltage was obtained with lower shot noise (which is the dominant error here) when R_F was increased to 10^9 ohm and the biasing voltage was decreased to 220V. In the first case, the multiplication factor was about 700, while in the second case it was about 300. However, the best standard deviation was 0.6% at an output voltage U_O = 0.5V, while in the case of the PN photodiodes, the standard deviation was 0.1% at the same output voltage during one measurement cycle of 13.3 minutes.

7. Design Conclusions

For low-level optical radiation measurements both PN and Avalanche silicon photodiodes can be used successfully. The application of avalanche diodes for highly stable and accurate measurements requires very high stability biasing high voltage sources and high precision temperature control. The elimination of the DC biasing voltage for the output of the short circuit current meter requires another compensating voltage source of similar characteristics. These are expensive and require large electronic or battery units which limit the technical performance. Otherwise, the sensitivity is limited by the shot noise of the avalanche diode. Higher sensitivity can be obtained with unbiased PN silicon photodiodes where the detector has only thermal noise. Here the

dominant error which is 1/f noise originates from the short circuit current measuring amplifier if the electrical bandwidth is properly decreased and the detector and amplifier are properly temperature controlled. The latter solution also does not require the extra power supplies.

REFERENCES

Bhardwaj, B. (1982). Silicon photodiodes - physics and technology. Report. United Detector Technology, Culver City, California, 37.

Borucki, W. J., (1984). Photometric precision needed for planetary detection. Proceedings of the NASA/SDSU Workshop on Improvements to Photometry, 15-27.

Borucki, W. J., and A. L. Summers (1984). The photometric method of detecting other planetary systems. **Icarus 58**, 121-134.

Borucki, W. J., L. E. Allen, S. W. Taylor, A. T. Young, and A. R. Schaefer (1987). A photometric approach to detecting earth-sized planets. Proceedings of the International Astronomical Union Colloquium No. 99: Bioastronomy - The Next Steps.

Eppeldauer, G. and Lanc, J. (1980). Problems of photocurrent measurements using photovoltaic cells. IMEKO 9th Intern. Symp. Photon-Detectors, Visegrad, Hungary, Proceedings Vol. 2. 310-316.

Eppeldauer, G. (1982) High sensitivity absolute radiometer. IMEKO 10th Intern. Symp. Photon-Detectors, Berlin (W), Proceedings 145-156.

Fisher, Richard (1968). P-I-N Diode Detectors for Astronomical Photometry. **Appl. Opt. 7**, 1079-1082.

Geist, J., E. Liang, and A. R. Schaefer (1981). Complete collection of minority carriers from the inversion layer in induced junction diodes. **J. Appl. Phys. 52**, 4879-4881.

Geist, J., E. F. Zalewski, and A. R. Schaefer (1980). Spectral response self-calibration and interpolation of silicon photodiodes. **Appl. Opt. 20**, 3795.

Schaefer, A. R., (1984). Photodiodes for astronomical stellar radiometry. Proceedings of the NASA/SDSU Workshop on Improvements to Photometry, 193-202.

Wilson, A. D. and H. Lyall (Dec, 1986). Design of an ultraviolet radiometer. 1: Detector electrical characteristics. **Appl. Opt. 25**, 4530-4539.

Zalewski, E. F. and J.C. Geist (1980). Silicon photodiode absolute spectral response self-calibration. **Appl. Opt. 19**, 1214-1216.

Table 1

SHUNT RESISTANCES OF LARGE SURFACE PHOTODIODES

IN DARK vs TEMPERATURE

Photovoltaic det.			Shunt resistance (Mohm)			Surface (mm^2)
Manufacturer	Type	No	25°C	30°C	35°C	
EG&G	UV 444 B	1-A	240	136	80	100
		2	71.5	-	35.2	100
		3	19.4	-	14.2	100
Hamamatsu	S 875-1010R	1	793.6	473	314	98
	S876-1010BQ	2	211.1	166.5	103.7	98
Hamamatsu	S1227-1010BQ	1	1950	-	-	98
		2	975	-	-	98
		3	2120	-	-	98
		4	1460	-	-	98
Hamamatsu	S1226-8BK	1-C	1433	840	474	33
		2	349.1	236.7	160.1	33
		3	2475.4	1183.9	640.7	33
		4	778	490.6	286.6	33

Table 2

IMPORTANT PARAMETERS OF OPERATIONAL AMPLIFIERS

SUITABLE FOR VERY LOW SHORT CIRCUIT CURRENT MEASUREMENT

Manufacturer	Type		Input bias pA	Voltage drift /uV/°C	Voltage noise .1-10Hz Vp-p	Current noise .1-10Hz fAp-p
Analog Devices	AD 545	J	2	25	3	10
		K	1	15	3	10
		L	1	5	3	10
		M	1	3	5	10
Analog Devices	AD 515	J	0.3	50	4	3
		K	0.15	15	4	3
		L	0.075	25	4	3
Burr Brown	3528	AM	0.3	±5 (±15)	6	7
		BM	0.15	±2 (± 5)	6	5
		CM	0.075	±5 (±10)	6	4
Burr Brown	3523	J	0.5	50	4	3
		K	0.25	25	4	3
		L	0.1	25	4	3
Burr Brown	OPA 104	AM	0.3	+15 (±25)	6	3
		BM	0.15	±10 (±15)	6	3
		CM	0.075	± 5 (±10)	6	3
Burr Brown	OPA 111	AM	+0.8(±2)	±2 (±5)	1.6 (3.3)	9.5 (15)
		BM	±0.5(±1)	±0.5(±1)	1.2 (2.5)	7.5 (12)
		SM	±0.8(±2)	±2 (±5)	1.6 (3.3)	9.5 (15)
Burr Brown	OPA 128	JM	+0.3	+20	4	4.2
		KM	±0.15	±10	4	3
		LM	±0.075	± 5	4	2.3
		SM	+0.15	±10	4	3

Table 3

THE PEAK-TO-PEAK NOISE VOLTAGES OF

FOUR BB OPA 111 OPERATIONAL AMPLIFIERS

Op. amp. No	Noise voltage /uVp-p
1	1
2	1
3	1.2
4	2.3

Table 4

OUTPUT ZERO ERRORS (Δf=0 to 0.1 Hz) vs TEMPERATURE

DETECTOR: 1-A; OPERATIONAL AMPLIFIER: TYPE 111

	Temperature (^{o}C)		
	25	30	35
Shunt resistance, Rs (Mohm)	240	136	80
Source resistance, Rr (Mohm)	229	132	78
Average noise voltage (V)	.00033	.00167	.00487
Standard deviation (V)	.00025	.00032	.00062
Minimum (V)	-.00025	.00066	.00325
Maximum (V)	.00098	.00266	.00622

Table 5

OUTPUT ZERO ERRORS (Δf= 0 to 0.1 Hz) vs TEMPERATURE

DETECTOR: 1-C; OPERATIONAL AMPLIFIER: TYPE 111

	Temperature (^{o}C)		
	25	30	35
Shunt resistance, Rs (Mohm)	1433	825	465
Source resistance, Rr (Mohm)	1113	708	425
Average noise voltage (V)	.00014	.00057	.00012
Standard deviation (V)	.00012	.00011	.00014
Minimum (V)	-.00014	.00031	-.00022
Maximum (V)	.00041	.00085	.00042

Table 6

OUTPUT ZERO ERRORS (Δ f= 0 to 0.1 Hz) vs TEMPERATURE

DETECTOR: 1-C; OPERATIONAL AMPLIFIER: TYPE 3523

	Temperature (^{o}C)		
	25	30	35
Shunt resistance, Rs (Mohm)	1433	840	474
Source resistance, Rr (Mohm)	1113	719	432
Average noise voltage (V)	.0004	.00037	.00059
Standard deviation (V)	.00007	.00017	.00023
Minimum (V)	.00021	.00025	-.00029
Maximum (V)	.00055	.00074	.0012

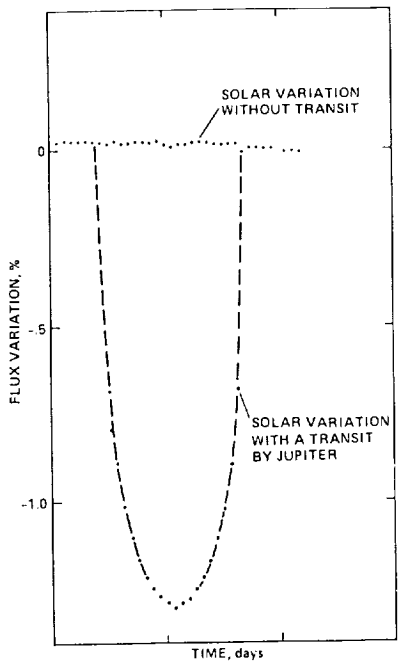

Fig. 1. Simulation of the flux variation of the sun due to a transit by Jupiter as seen by a distant observer.

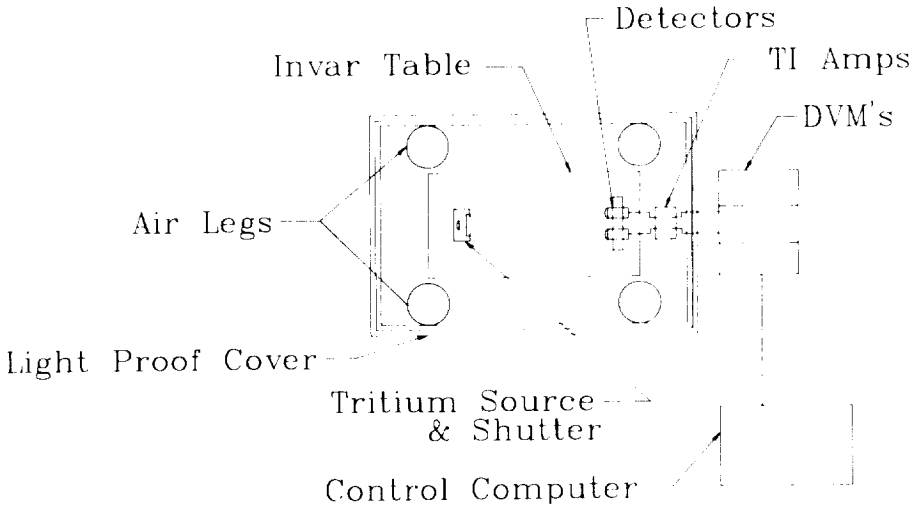

Fig. 2. Block diagram of low light level characterization facility.

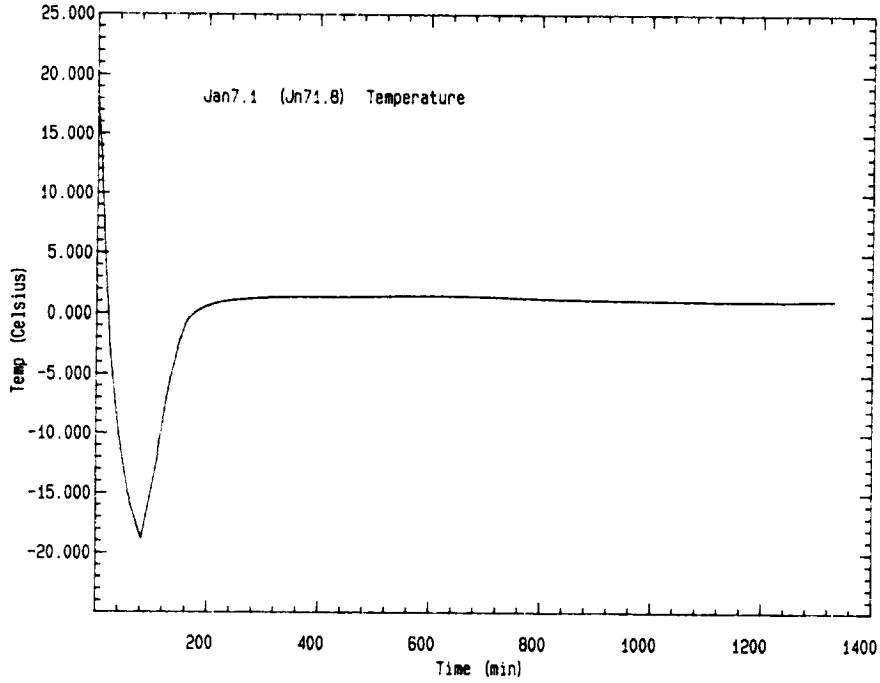

Fig. 3. Temperature vs. time of high gain transimpedance amplifier test.

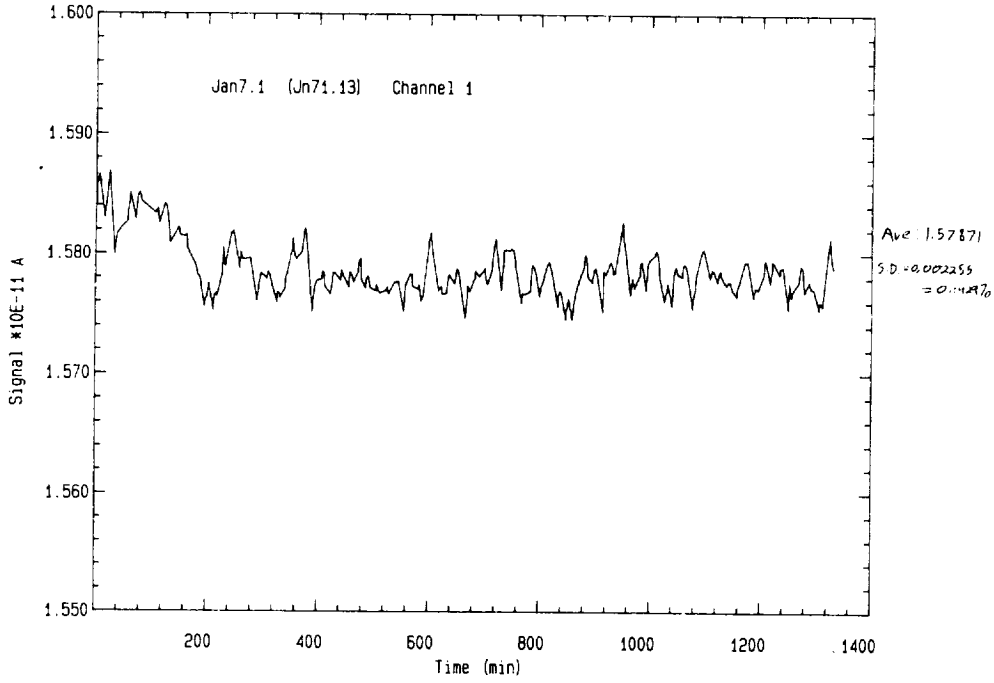

Fig. 4. Channel 1 Signal vs. time of silicon photodiode amplified photocurrent during temperature cycle.

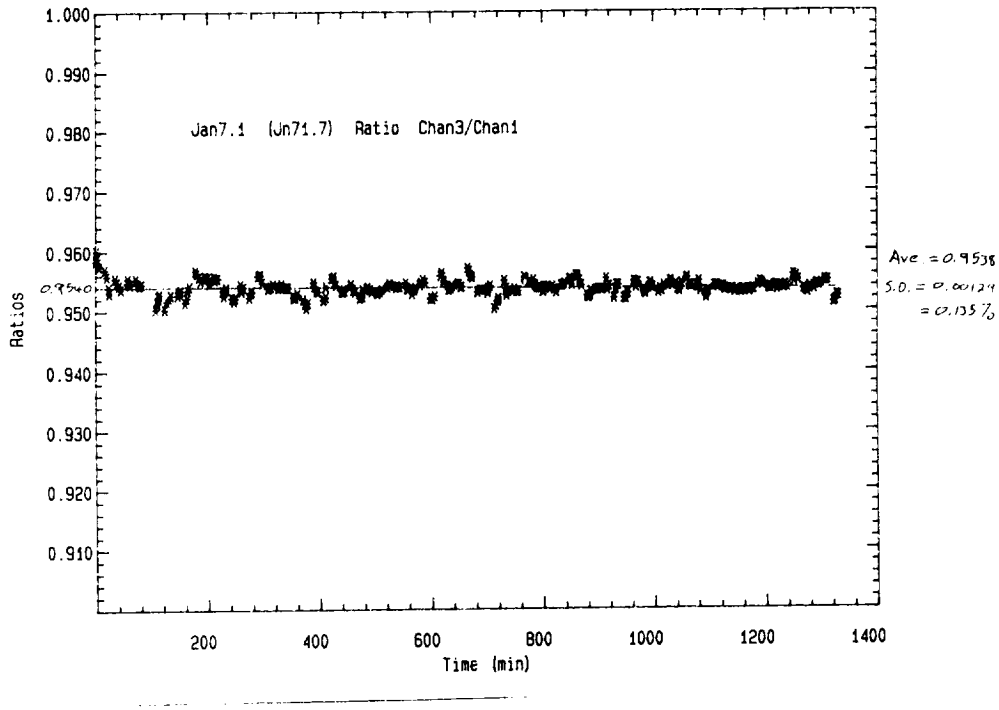

Fig. 5. Channel 3/Channel 1 Signals ratioed vs. time during temperature cycle.

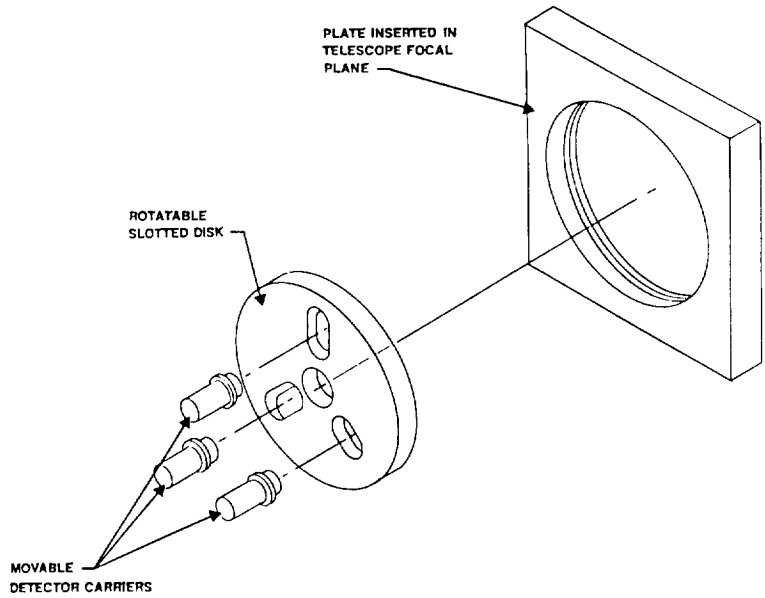

Fig. 6. Diagram of breadboard photometer used at the Lick Observatory Twin Astrograph.

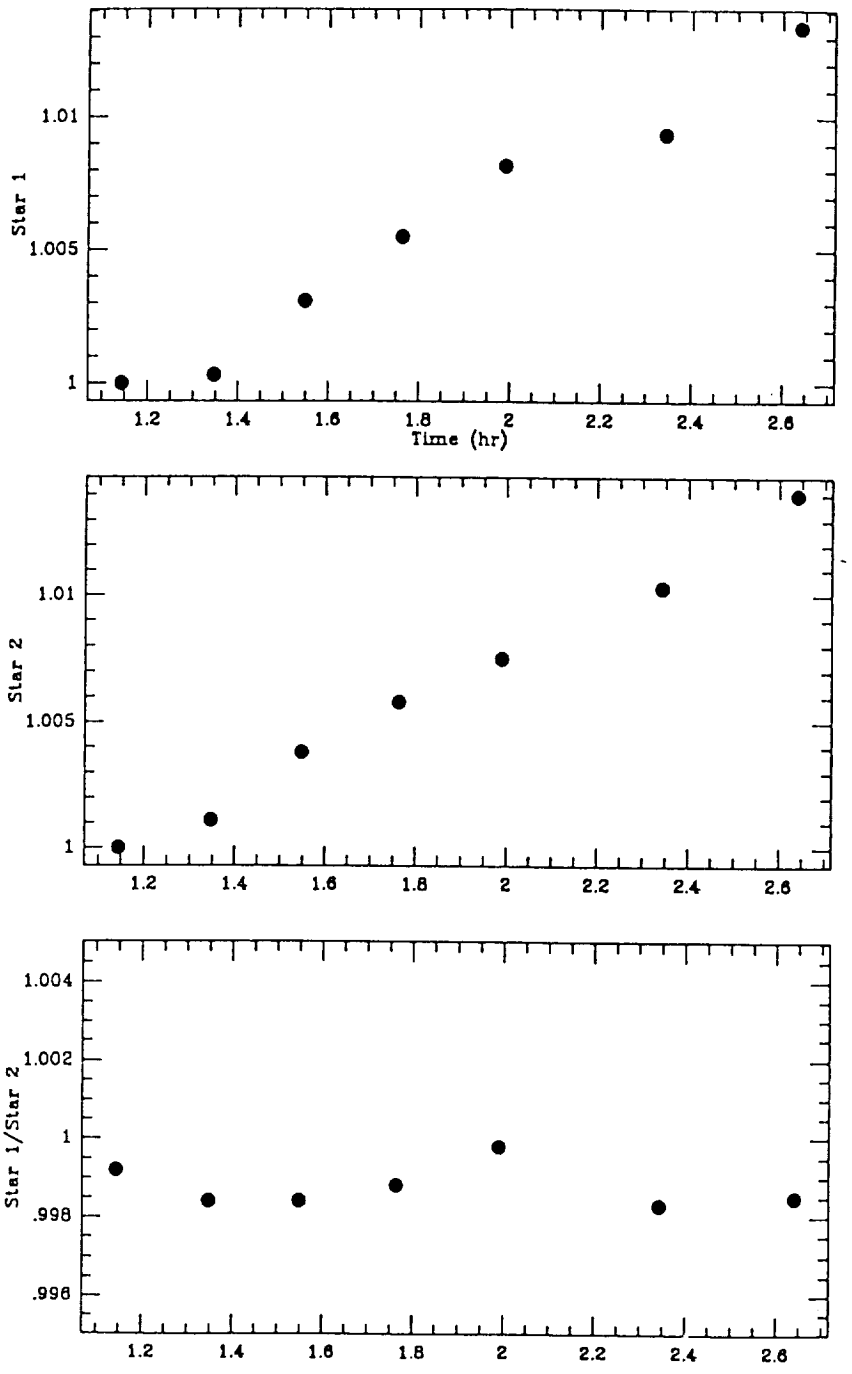

Fig. 7. The variation of the brightness of two stars and the ratio of their brightness as a function of time. Star 1 is alpha-Aries and star 2 is beta-Aries.

ORIGINAL PAGE IS
OF POOR QUALITY

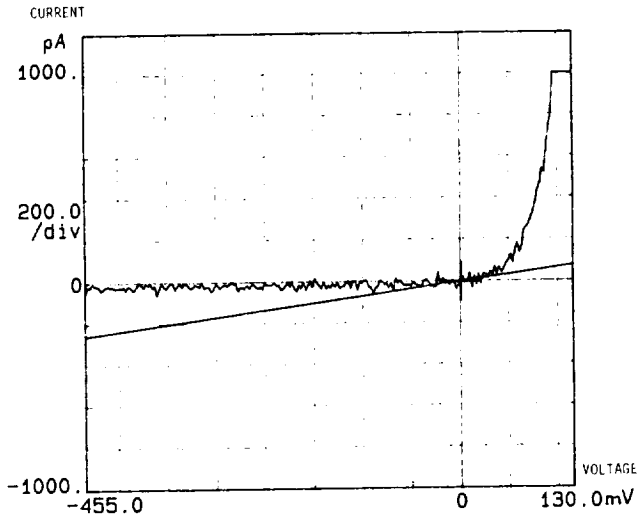

Fig. 8. Current-voltage characteristic of a 1 cm^2 surface Hamamatsu photodetector Model 1227-1010 BQ.

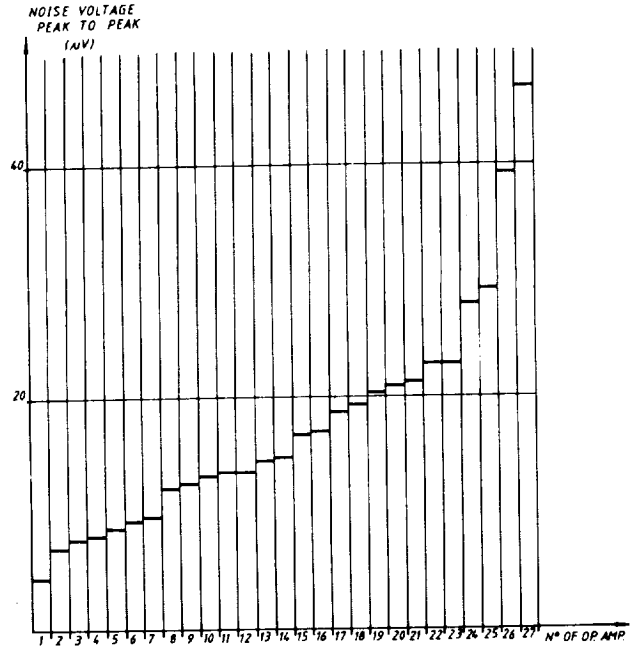

Fig. 9. The peak to peak noise voltages of 27 AD 515 and BB 3523 operational amplifiers.

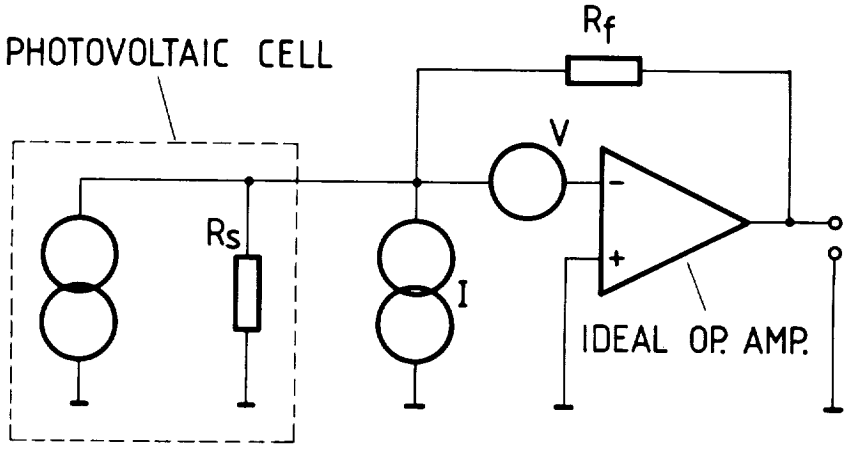

Fig. 10. Simplified equivalent circuit of the light measuring circuit.

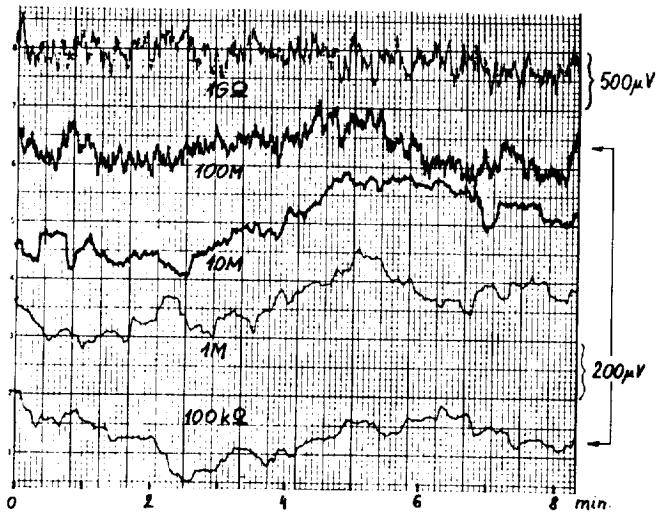

Fig. 11. The total noise output voltages of the operational amplifier 3523 type at different source resistance values and constant amplification of 50.

ORIGINAL PAGE IS
OF POOR QUALITY

ORIGINAL PAGE IS
OF POOR QUALITY

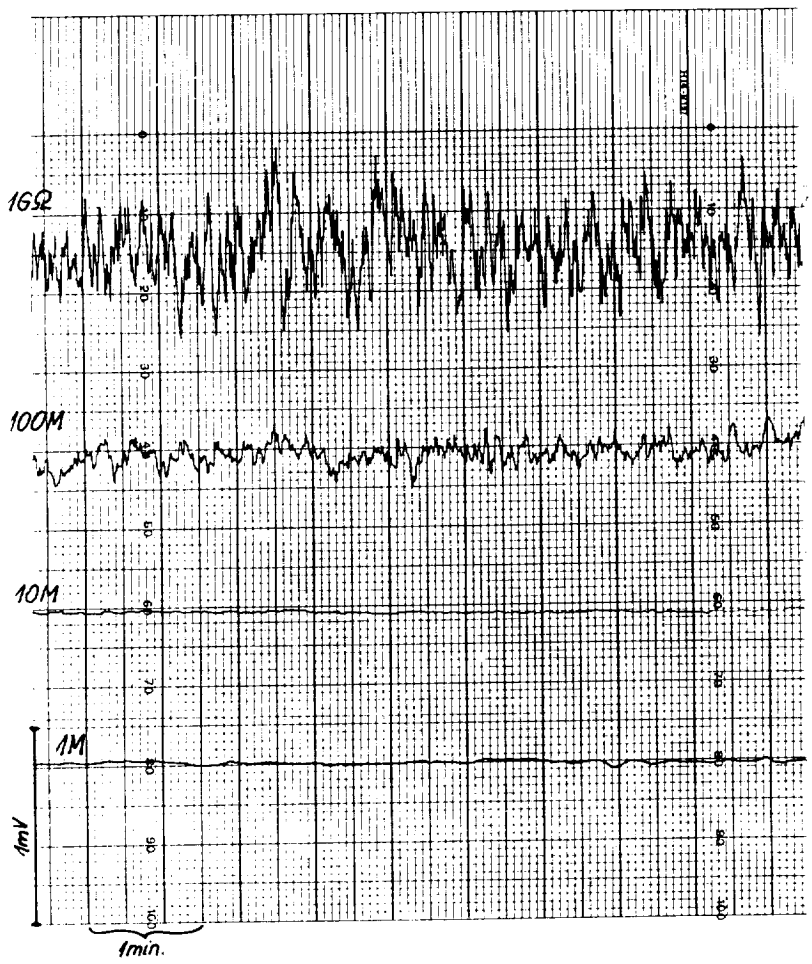

Fig. 12. The total noise output voltages of the operational amplifier 111 type at different source resistance values and constant amplification of 50.

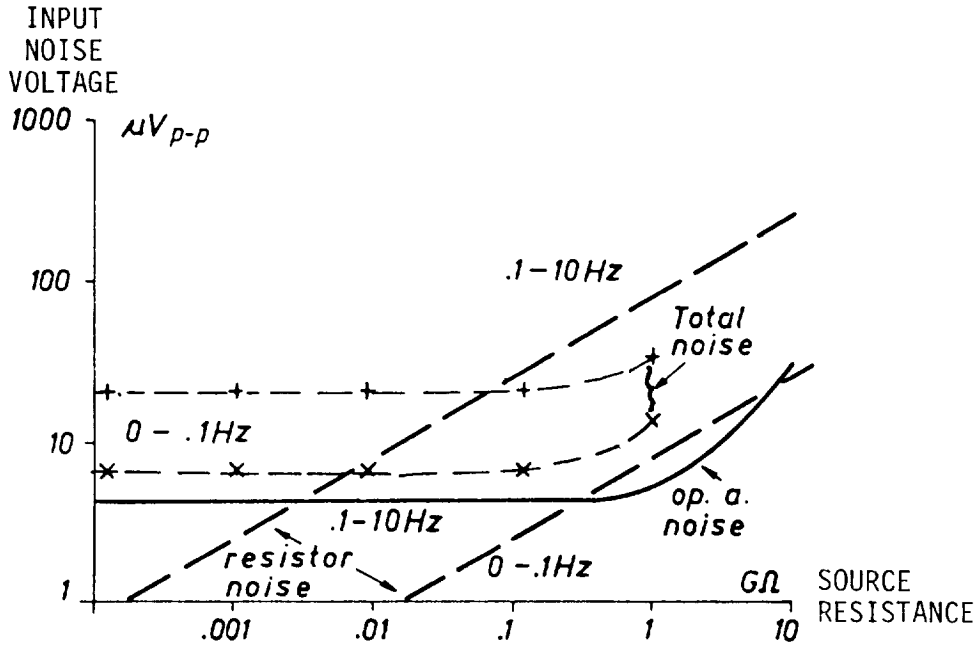

Fig. 13. Input noise voltages of the operational amplifiers 3523 type vs. source resistance.

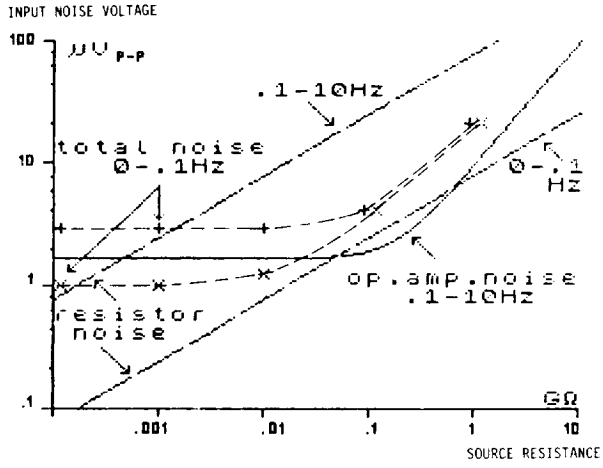

Fig. 14. Input noise voltages of operational amplifiers 111 type vs. source resistance.

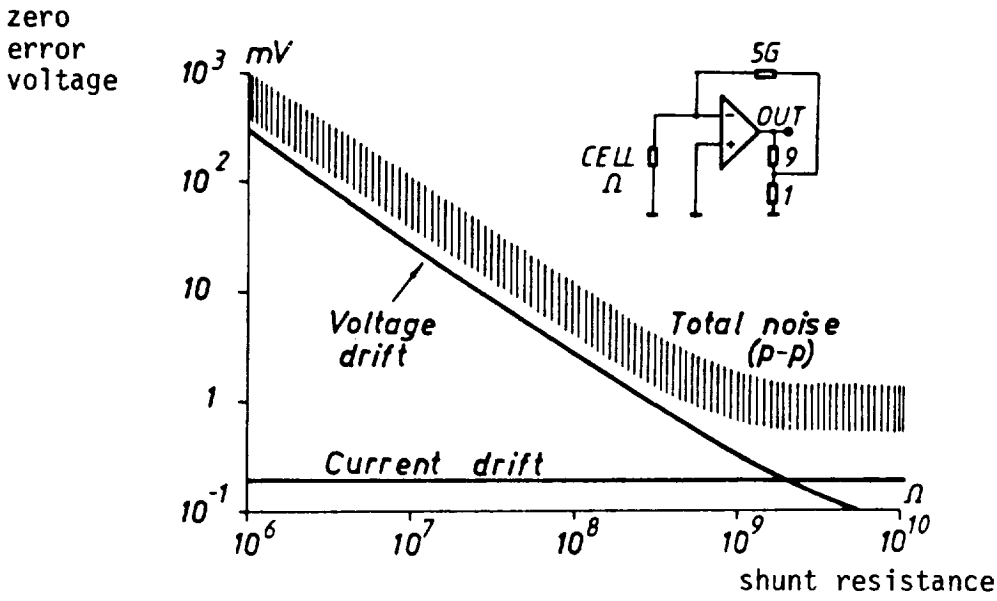

Fig. 15. Output zero error voltages of operational amplifiers 3523 type vs. shunt resistance.

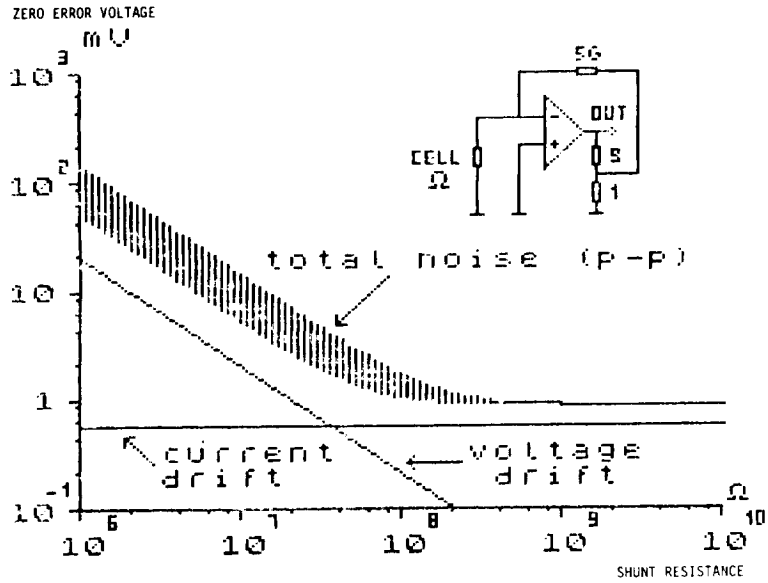

Fig. 16. Output zero error voltages of operational amplifiers 111 type vs. shunt resistance.

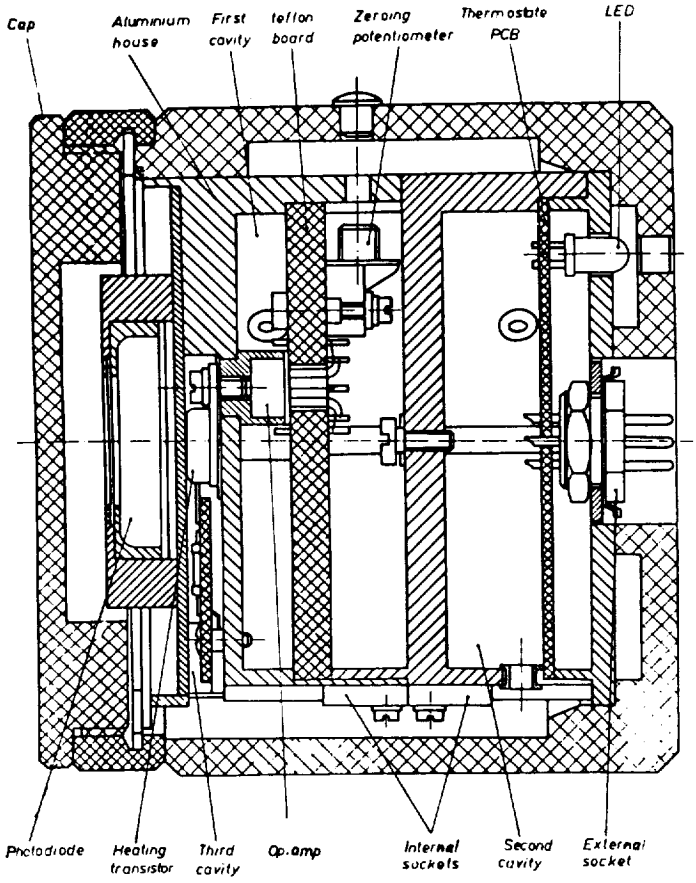

Fig. 17. Temperature controlled high sensitivity light measuring head.

ORIGINAL PAGE IS
OF POOR QUALITY

ORIGINAL PAGE IS
OF POOR QUALITY

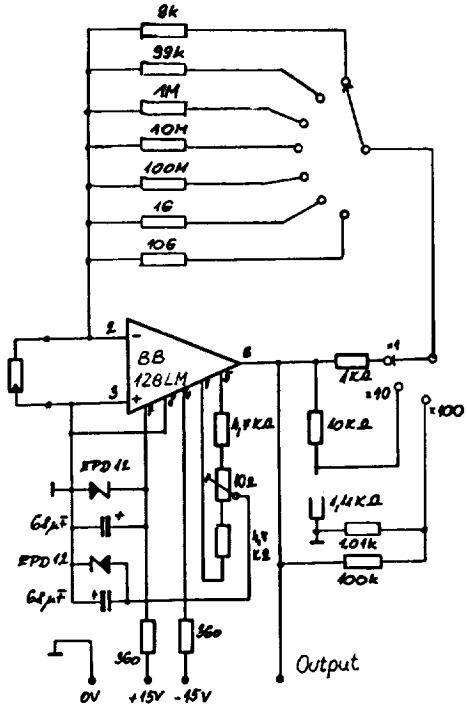

Fig. 18. Multi-range short circuit current to voltage converter.

ORIGINAL PAGE IS
OF POOR QUALITY

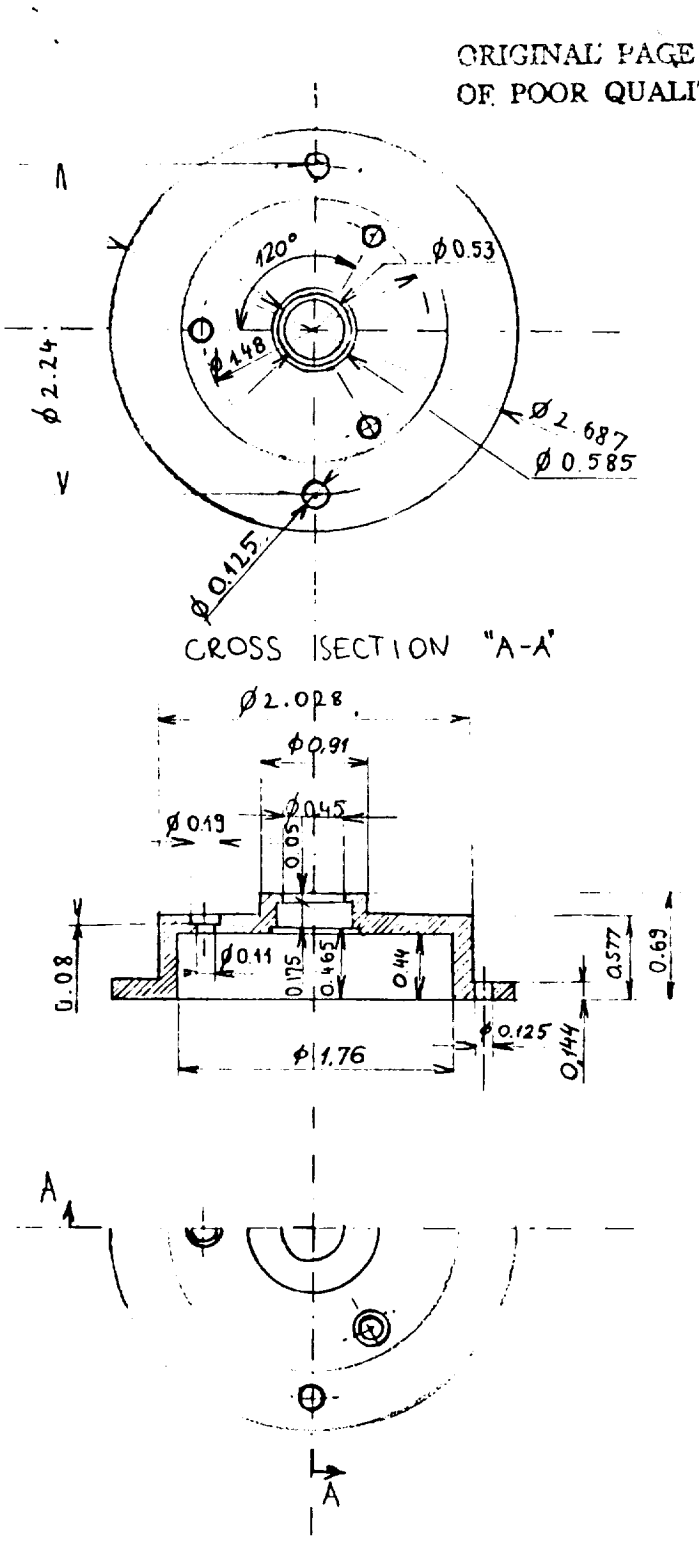

Fig. 19. Silicon avalanche photodiode adaptor for the temperature controlled measuring head.

ORIGINAL PAGE IS
OF POOR QUALITY

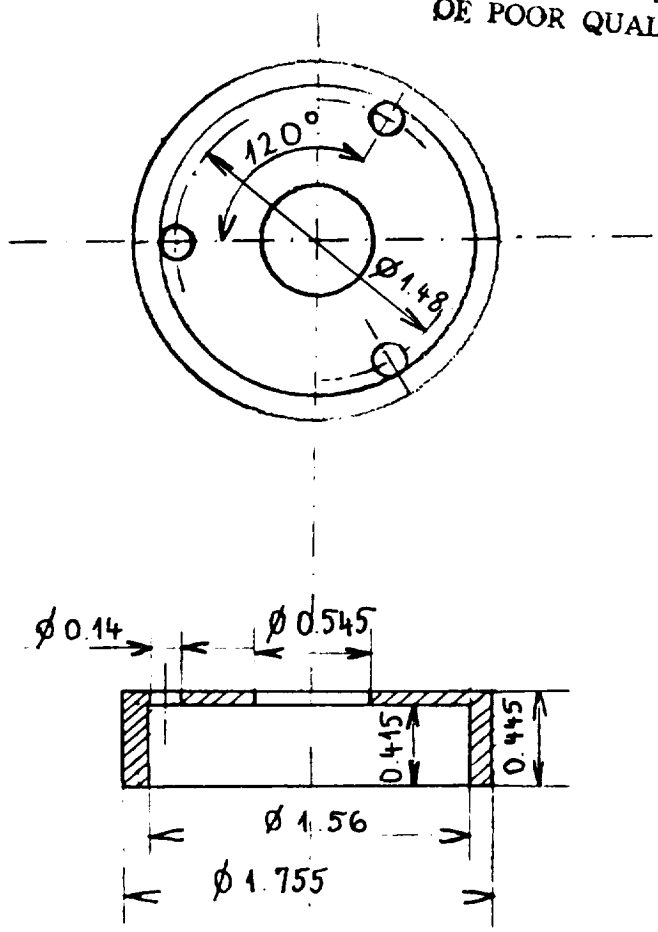

Fig. 20. Silicon avalanche photodiode inside adaptor for the temperature controlled measuring head.

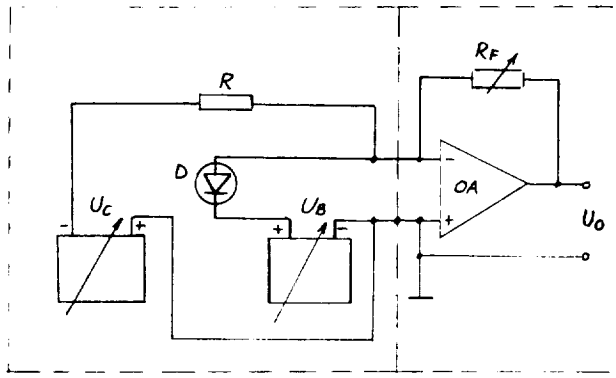

Fig. 21. High voltage biasing circuit of the silicon avalanche photodiode.